

Interannual and Interdecadal Variability in the Storm Track, Cloudiness, and Sea Surface Temperature over the Summertime North Pacific

JOEL R. NORRIS

National Center for Atmospheric Research, Boulder, Colorado*

(Manuscript received 18 September 1998, in final form 12 March 1999)

ABSTRACT

Interannual and interdecadal variability in the summertime mean North Pacific storm track is examined in relation to summertime mean sea surface temperature (SST), nimbostratus, and marine stratiform cloudiness (MSC) (stratus, stratocumulus, fog). The storm track is diagnosed by root-mean-squared daily vertical velocity at 500 mb during the summer season (rms ω) obtained from the National Centers for Environmental Prediction–National Center for Atmospheric Research reanalysis. The cloud and SST data are obtained from surface observations. Year-to-year variations in the storm track exhibit significant coupling to variations in cloudiness and SST across the North Pacific. These correspond to coincident latitudinal shifts in the storm track, SST gradient, and MSC gradient. Moreover, both rms ω and nimbostratus show that the storm track moved equatorward and intensified between 1952 and 1995, consistent with the previously documented upward trend in MSC and downward trend in SST. Lead–lag relationships suggest variability in the storm track has a large role in forcing variability in SST. Boundary layer cloudiness responds to and adds a positive feedback to variability in SST.

Weak relationships are observed with the summertime mean large-scale circulation, as diagnosed by sea level pressure. This suggests summertime North Pacific atmosphere–ocean interaction is dominated by local processes operating in the storm track and over the SST gradient, unlike the situation during winter.

1. Introduction

Cloudiness is one of the most important variables influencing the earth's radiation budget, but its role in global climate system is not well understood. Since current general circulation models do not consistently and correctly simulate cloudiness (Cess et al. 1996; Weare et al. 1996), observational studies have been undertaken to investigate variability in cloudiness over the extratropical ocean on interannual and longer timescales (e.g., Hanson 1991; Klein et al. 1995; Norris and Leovy 1994; Norris et al. 1998; Weare 1994). These investigations have primarily examined relationships between sea surface temperature (SST) and cloudiness in the marine boundary layer. For example, Norris et al. (1998; hereafter NZW) examined interannual and interdecadal variability in marine stratiform cloudiness (MSC; stratus, stratocumulus, and fog) and SST over the summertime North Pacific between 1952 and 1992. Using empirical orthogonal function analysis and singular val-

ue decomposition analysis, they found that seasonal anomalies in MSC amount tend to be negatively correlated with seasonal SST anomalies, particularly in the central and western Pacific along 35°N (NZW, Fig. 5). This region coincides with strong meridional gradients in climatological SST and MSC amount, and interannual anomalies reflect year-to-year coupled latitudinal shifts in the gradient locations. Along with short-term variability, a long-term decrease in SST and increase in MSC amount occur during the 1952–92 time period. These results are suggestive of a positive cloud feedback on SST, where increased cloud amount acts to cool the ocean by decreasing surface insolation and decreased SST favors greater MSC amount through boundary layer processes described in Norris (1997) (hereafter N97).

NZW also examined relationships between seasonal anomalies of sea level pressure (SLP) and MSC and SST over the summertime North Pacific. Colder SST and greater MSC amount in the central North Pacific are associated with a slight weakening of the northwest flank of the seasonal mean subtropical anticyclone (NZW, Figs. 6 and 7), but coupling between SST and SLP is weak. This lack of connection with the seasonal mean large-scale circulation is in distinct contrast to the situation during winter, when SST anomalies exhibit substantially stronger coupling to the Pacific–North America pattern, the dominant mode of low-frequency

* The National Center for Atmospheric Research is sponsored by the National Science Foundation.

Corresponding author address: Joel R. Norris, NCAR/ASP, P.O. Box 3000, Boulder, CO 80307-3000.
E-mail: jnorris@ucar.edu

atmospheric variability in this sector (Wallace et al. 1992).

The weak organization of summertime atmospheric circulation over the North Pacific favors the view that summertime midlatitude atmosphere–ocean interaction predominantly occurs between atmospheric and oceanic boundary layers, but there is evidence to the contrary. Norris and Leovy (1994) (hereafter NL94) found that local correlations between seasonal anomalies of nimbostratus and SST are nearly as high as correlations between MSC amount and SST over the central and western North Pacific during summer. Although these correlations suggested the occurrence of coincident latitudinal shifts of the storm track and the SST gradient, it was not clear how much of the surface-observed nimbostratus was merely thickened boundary layer stratus because the data used by NL94 (Warren et al. 1988) included an unknown contribution from drizzle reports. As an alternative, N97 investigated interannual shifts in the storm track between 1954 and 1992 using seasonal variance of daily surface geostrophic meridional wind component estimated from SLP analyses. Unfortunately, results were marginal due to changes in analysis procedure over the time period.

It is important to establish whether changes in the location and strength of the summertime storm track are related to changes in SST and cloudiness in order to understand what cloud processes and cloud feedbacks over the midlatitude ocean are significant. NZW suggested positive feedback between SST and boundary layer cloudiness contributes to the persistence of SST anomaly patterns through the summer season despite the low thermal inertia of the shallow summertime ocean mixed layer. This picture becomes more complex if it is necessary to consider changes in surface forcing related more to synoptic activity than to a simple boundary layer response to SST. Weaver and Ramanathan (1996) have demonstrated that cloudiness associated with extratropical cyclones produces the strongest radiative forcing over the summertime North Pacific. Furthermore, extratropical cyclones produce greater surface stress and surface heat flux. The present study extends the work of NZW by examining interannual and interdecadal variability in the storm track, cloudiness, and SST over the summertime North Pacific. The storm track is diagnosed by a new surface-observed nimbostratus dataset that excludes drizzle and by a dynamical measure of synoptic activity obtained from the recently completed National Centers for Environmental Prediction–National Center for Atmospheric Research (NCEP–NCAR) reanalysis project.

2. Data and analysis procedures

The time period examined by the present study is 1952–95. Results are presented for the summer season, defined as June–August (JJA). The winter season, de-

finied as December–February, was also analyzed, but no results are shown.

Cloud data were obtained from the raw dataset of surface synoptic observations used by NZW, now updated through 1995. The same method was used to calculate mean MSC amount, except the $2.5^\circ \text{ lat} \times 5^\circ \text{ long}$ averages were aggregated to a regular $5^\circ \text{ lat} \times 10^\circ \text{ long}$ grid instead of a $10^\circ \text{ lat} \times 20^\circ \text{ long}$ grid. The disadvantage of greater sampling noise is outweighed by the advantage of better spatial resolution. Nimbostratus was diagnosed following Hahn et al. (1996), except no drizzle reports were allowed to contribute. To avoid assumptions about upper-level cloud cover when low-level cloud cover is overcast, nimbostratus frequency-of-occurrence (FQ) was used instead of nimbostratus cloud amount (the presence of nimbostratus can always be identified by the occurrence of precipitation). There is little difference between the two since nimbostratus is almost always overcast when it occurs. Nimbostratus FQ was averaged to JJA means and a $5^\circ \times 10^\circ$ grid in the same manner as for MSC amount. Only daytime (including twilight) observations were used to calculate MSC amount and nimbostratus FQ because observers sometimes have difficulty identifying cloudiness under conditions of poor illumination (Hahn et al. 1995; Rozendaal et al. 1995).

SST data were obtained from the *Global Ocean Surface Temperature Atlas* (Bottomley et al. 1990), updated through 1995. The $5^\circ \times 5^\circ$ monthly means were averaged to $5^\circ \times 10^\circ$ JJA means. This dataset produces very similar results to the Comprehensive Atmosphere–Ocean Data Set (COADS; Woodruff et al. 1987) used by NZW. SLP data were obtained from the NCEP–NCAR reanalysis project (Kalnay et al. 1996) and produce very similar results to the COADS SLP used by NZW. Monthly $2.5^\circ \times 2.5^\circ$ means were averaged to JJA $5^\circ \text{ lat} \times 10^\circ \text{ long}$ means. Because the reanalysis grid is offset from the grid used by the SST and cloud data, the centerpoints of the SLP $5^\circ \text{ lat} \times 10^\circ \text{ long}$ grid boxes are 1.25° north and 1.25° west of the centerpoints of the SST and cloud $5^\circ \text{ lat} \times 10^\circ \text{ long}$ grid boxes.

The mean location and intensity of synoptic activity during JJA was diagnosed by the root-mean-squared daily pressure vertical velocity (ω) at 500 mb (hereafter referred to as rms ω). A 3–30-day bandpass filter was applied to daily mean ω using a 121-point weighted running mean. Most of the power is at synoptic time-scales, as would be expected for vertical velocity. The seasonal mean was subtracted from the filtered daily means, and the resulting daily deviations were used to calculate rms ω during JJA. The $2.5^\circ \times 2.5^\circ$ means were averaged to $5^\circ \text{ lat} \times 10^\circ \text{ long}$ means on the same grid as for SLP. Rms ω was chosen as a measure for synoptic activity because the occurrence of nimbostratus is closely related to midtropospheric vertical velocity and because Weaver and Ramanathan (1997) note that summertime shortwave cloud radiative forcing is greatest where rms ω is greatest. Large rms ω is associated with

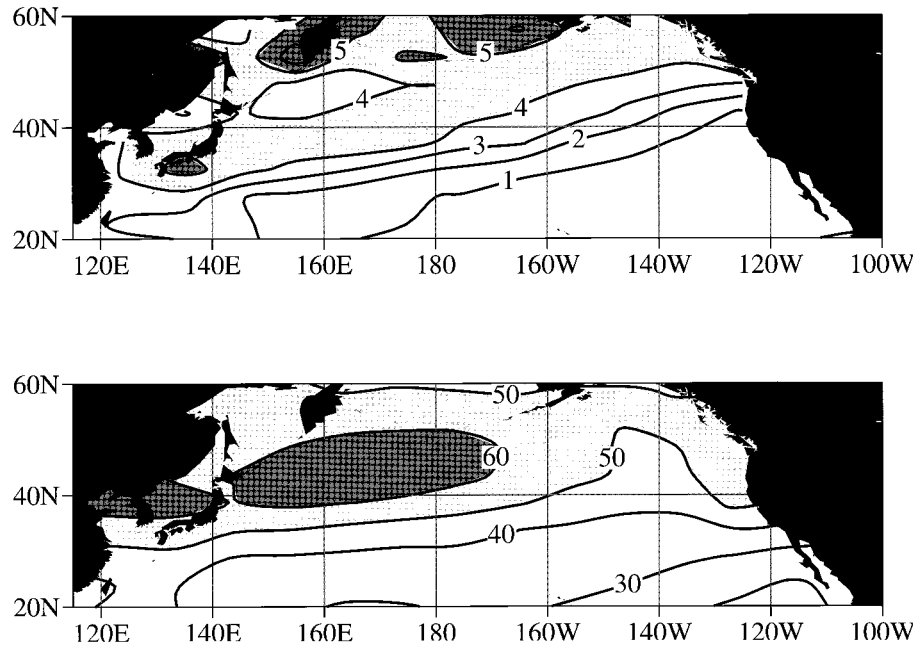


FIG. 1. (a) Climatological JJA daytime nimbostratus FQ. Contour interval is 1%; threshold for lighter (darker) shading is 4% (5%). (b) Climatological JJA rms ω . Contour interval is 10 mb day⁻¹; threshold for lighter (darker) shading is 50 mb day⁻¹ (60 mb day⁻¹).

a greater frequency of strong ascent and hence the more frequent occurrence of thick, high-albedo frontal clouds.

Following NZW, empirical orthogonal function (EOF) analysis and singular value decomposition (SVD) analysis (Bretherton et al. 1992) were used to identify the dominant spatial patterns associated with interannual and interdecadal variability in the parameters. The domain for the EOF and SVD analyses was chosen to be 25°–60°N to focus on midlatitude processes. Regions west of 140°E and east of 120°W were excluded from the domain to avoid cloud variability due to offshore flow. The Bering Sea and the Sea of Okhotsk were also excluded to avoid spurious cloud variability arising from the low sampling density. The results are not sensitive to these limitations of the domain. SVD statistics for describing the strength of coupling between two fields are squared covariance fraction (SCF), normalized root-mean-squared covariance (NC), and the correlation between the expansion coefficient time series of the left and right fields of an SVD mode (r). The NC, defined in Zhang et al. (1998) (hereafter ZNW), is introduced to more directly compare the strength of relationship between left and right fields obtained from different SVD analyses. Statistical significance was calculated by a Monte Carlo method taking autocorrelation into account that is described in the appendix.

EOF and SVD analysis results are presented by regressing the fields on the normalized expansion coefficient time series; hence, the contoured values represent typical anomalies. In the terminology of Bretherton et

al. (1992), the fields presented from SVD analysis are heterogeneous regression patterns.

3. Results

Climatological nimbostratus FQ and rms ω over the summertime midlatitude North Pacific are displayed in Fig. 1. This nimbostratus climatology is generally similar to that of Warren et al. (1988) but has smaller values due to the exclusion of drizzle observations. The nimbostratus band seen in Fig. 1 stretching east from Japan coincides with climatological bands of surface-observed bad weather stratus (a low cloud type) (Norris 1998) and enhanced cloud liquid water path (Weng et al. 1997). Rms ω exhibits a maximum located poleward of the nimbostratus band. For conciseness climatologies of summertime North Pacific SST and MSC amount will not be displayed but instead can be found in NL94's Fig. 2 (SST) and their Fig. 1 (MSC amount).

Figure 2 displays the leading EOF patterns of nimbostratus FQ and rms ω , and Table 1 lists the variance explained. The EOF patterns of both parameters exhibit banded structures with centers of action slightly equatorward of the climatological maxima, confirming the existence of year-to-year latitudinal shifts in the location and intensity of the summertime storm track. It is interesting to note that the amplitude of the leading summertime rms ω EOF is as strong as the amplitude of the leading wintertime EOF despite the fact that climatological wintertime rms ω is almost twice as strong

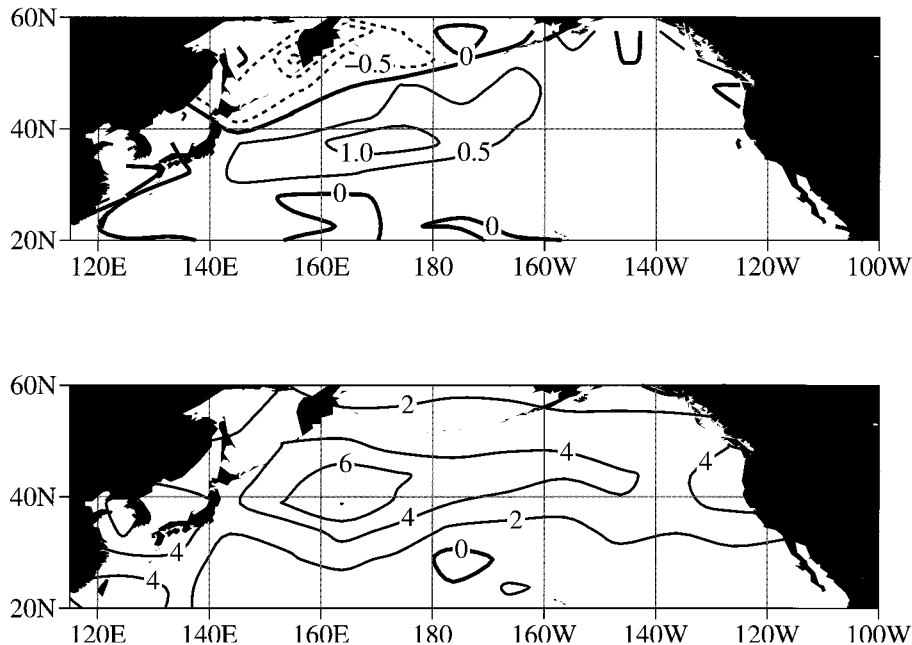


FIG. 2. Leading EOF patterns for (a) JJA daytime nimbostratus FQ and (b) JJA rms ω . Contour intervals are 0.5% and 2 mb day⁻¹; the zero contour is thickened and negative contours are dashed.

(not shown). Although the present study examines a slightly different period of record than the papers of ZNW and NZW (1952–95 instead of 1952–92), the leading EOF patterns for SST and SLP are nearly identical to ZNW's Fig. 4b (SST) and NZW's Fig. 8 (SLP) and thus will not be displayed. The leading EOF pattern for MSC amount (not shown) has a more zonally elongated central North Pacific center of action but weaker eastern subtropical North Pacific center of action than does NZW's Fig. 3. This difference probably results from analyzing a domain north of 25°N instead of 10°N.

Normalized time series corresponding to the leading EOFs are plotted in Fig. 3 for all parameters. Considerable correspondence is evident in the time series for nimbostratus FQ, rms ω , MSC amount, and SST, and correlations between them are all statistically significant (Table 2). Less correspondence is evident in the SLP time series, and correlations between SLP and the other parameters are much weaker. Generally upward trends exist in all time series except SLP. These correspond to an increase in nimbostratus FQ, an increase in rms ω , an increase in MSC amount, and a decrease in SST across the North Pacific in the vicinity of 40°N. These

are in qualitative agreement with trends calculated at single grid points for nimbostratus (including drizzle), MSC amount, and SST (NL94; Norris and Leovy 1995). The equatorward shift of the storm track is consistent with the decreasing trend in 500-mb geopotential height over the summertime midlatitude North Pacific documented by Reiter and Westhoff (1982) and Shabbar et al. (1990).

To investigate coupling between the summertime storm track and SST more closely, SVD analysis was conducted on nimbostratus FQ paired with SST (Fig. 4) and rms ω paired with SST (Fig. 5). The temporal behavior of the SVD expansion coefficient time series

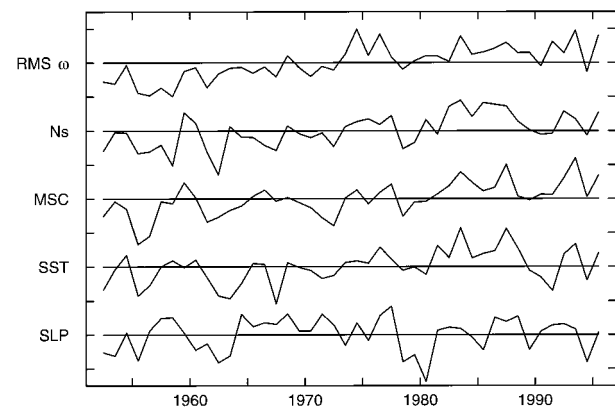


FIG. 3. Normalized time series for leading JJA EOFs of (top to bottom) rms ω , daytime nimbostratus FQ, daytime MSC amount, SST, and SLP. Tick marks on the ordinate scale are at intervals of two standard deviations.

TABLE 1. Variance explained by the first and second EOFs.

Parameter	EOF 1 (%)	EOF 2 (%)
Nimbostratus FQ	13.1	10.3
Rms ω	29.1	9.8
MSC amount	19.1	13.2
SST	26.4	18.3
SLP	35.1	17.4

TABLE 2. Correlation between EOF time series. Bold indicates 95% significance. Units are percent.

	Rms ω	MSC amount	SST	SLP
Nimbostratus FQ	72	73	66	21
Rms ω		73	60	23
MSC amount			71	34
SST				37

(not shown) can be inferred from the EOF expansion coefficient time series in Fig. 3. The patterns presented in Fig. 4 resemble the leading EOFs for nimbostratus FQ (Fig. 2) and SST (ZNW, their Fig. 4b). An equatorward shift of the nimbostratus band is associated with an equatorward shift of the SST gradient. Figure 5 displays a similar equatorward shift and intensification of rms ω . This pattern resembles that for the leading EOF (Fig. 2). Statistics for the SVD analyses (listed in Table 3) indicate significant coupling between the storm track and SST. Because apparent coupling can be generated by the coincident trends in the fields, SVD analysis was performed on data that had been detrended using the year-to-year difference method described in NZW. Similar spatial patterns result, and the correlation of SVD expansion coefficient time series increases (nimbostratus–SST $r = 83$; rms ω –SST $r = 82$).

Statistically significant coupling also exists between the summertime storm track and MSC amount (Table 3). While this might be expected for MSC and nimbostratus (since the low clouds that commonly occur under nimbostratus contribute to MSC), it is also the

case for MSC and rms ω . Figure 6 presents the SVD patterns for MSC amount paired with rms ω . An equatorward shift in the MSC gradient across nearly the entire North Pacific is associated with an equatorward shift of the storm track. Summertime midlatitude MSC and SST variations are very strongly coupled, as indicated by Table 3. The SVD patterns (not shown) are similar to those displayed in NZW's Fig. 5, except excluding the subtropics from the SVD domain leads to a weaker eastern subtropical center of action than seen in NZW's Fig. 5. SVD analysis on the detrended fields shows that coupling with MSC is even stronger when the interdecadal variability has been removed (MSC–SST $r = 92$; MSC–rms ω $r = 85$).

The weak and largely nonsignificant SLP statistics in Tables 2 and 3 indicate the mean large-scale surface circulation plays little role in variability over the summertime midlatitude North Pacific (SVD patterns not shown). The dramatic drop in MSC–SLP coupling strength from NZW (SCF/NC/ $r = 62/18/82$) to the present study (SCF/NC/ $r = 48/14/66$) is attributed to confining the SVD domain to latitudes poleward of 25°N. Variability in summertime SLP over the North Pacific is dominated by variability in the subtropical anticyclone, and boundary layer cloudiness over the western and central North Pacific is less affected by the subtropical anticyclone than boundary layer cloudiness over the eastern subtropical North Pacific. The absence of a long-term trend in the SLP field may account for part of the lack of coupling since stronger correlations are obtained for SVD pairs of SLP with the other parameters when using detrended data ($r = 70$ to 77).

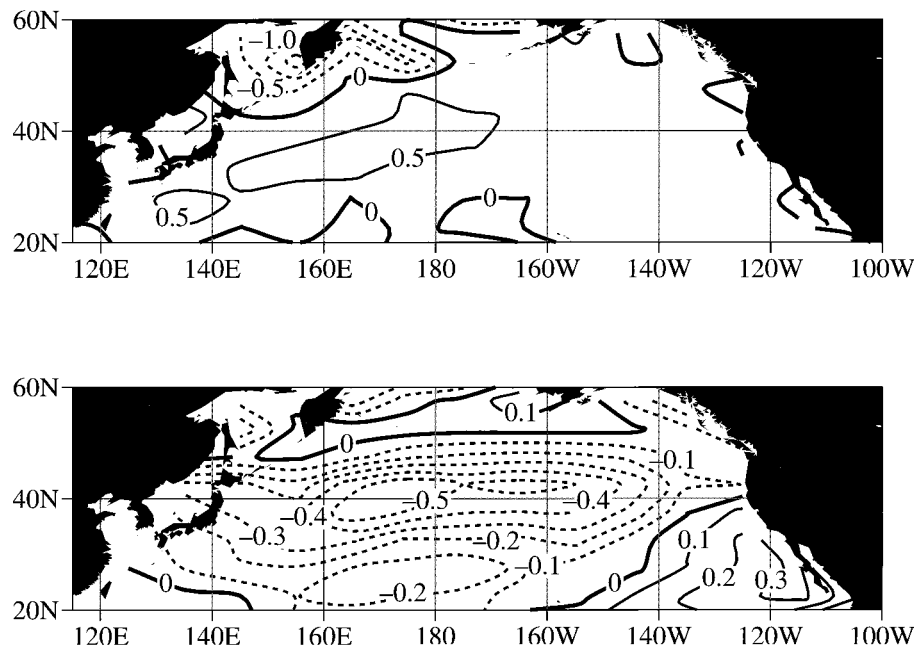


FIG. 4. Leading SVD patterns for (a) JJA daytime nimbostratus FQ paired with (b) JJA SST. Contour intervals are 0.5% and 0.1°C; the zero contour is thickened and negative contours are dashed.

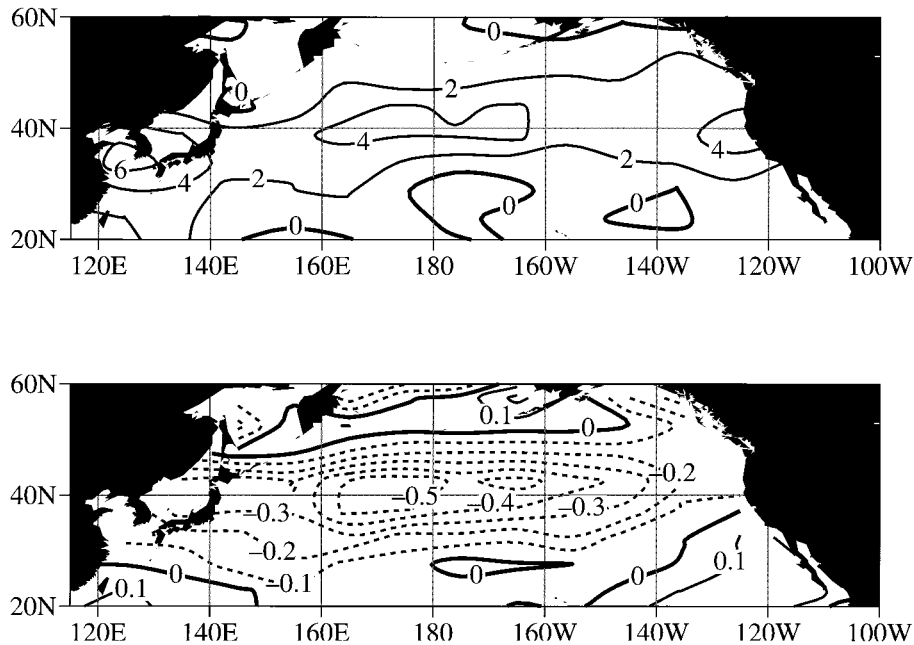


FIG. 5. Leading SVD patterns for (a) JJA RMS ω paired with (b) JJA SST. Contour intervals are 2 mb day^{-1} and 0.1°C ; the zero contour is thickened and negative contours are dashed.

Nevertheless, these values are still less than those obtained for detrended SVD pairs not including SLP.

4. Discussion

The EOF and SVD analysis results presented in the previous section demonstrate that interannual and interdecadal variability in the location and intensity of the summertime storm track is related to large-scale variability in North Pacific SST, but the precise nature of this coupling is more difficult to determine. Modeling studies evaluating the influence of midlatitude SST anomalies on wintertime atmospheric circulation (e.g. Ferranti et al. 1994; Kushnir and Held 1996; Lau and Nath 1990, among others) have produced ambiguous results. Some provide evidence that the storm track shifts equatorward in response to cold SST anomalies and poleward in response to warm SST anomalies, but the sensitivity of atmospheric circulation to midlatitude SST anomalies is weak. The very few modeling studies evaluating the influence of midlatitude SST anomalies on summertime atmospheric circulation (e.g. Lau and

Nath 1990) indicate the atmospheric response is even weaker.

The influence of storm track variability on SST has a more solid basis. Increased synoptic activity is associated with increased latent and sensible heat fluxes due to more frequent northerly advection and greater wind speeds (N97). These act to produce a cold SST anomaly. Increased synoptic activity is also associated with reduced surface insolation due to greater upper-level cloudiness (Weaver and Ramanathan 1996, 1997), which acts to produce a cold SST anomaly. Moreover, stronger winds associated with extratropical storms can create increased mechanical turbulence and entrain cold water from below into the ocean mixed layer. However, it is beyond the scope of the present study to quantitatively evaluate the impacts of cloud radiative forcing, latent and sensible heat fluxes, surface wind stress, and ocean mixed layer processes on summertime SST.

The impact of the storm track on SST variability can be explored with lead-lag correlations. Figure 7 shows that the springtime anomaly pattern of rms ω is closely related to the summertime anomaly pattern of SST and the summertime anomaly pattern of rms ω is closely related to the autumnal anomaly pattern of SST. This provides credence to the view that shifts in the storm track have a large role in producing shifts in the SST gradient. The fact that the correlation between simultaneous rms ω and SST is as great as the correlation when rms ω leads SST suggests that the storm track may in turn respond to SST anomalies. An alternative but not mutually exclusive explanation is that the shallowness of the summertime ocean mixed layer (20–30

TABLE 3. SVD statistics as described in section 2 (SCF/NC/ r). Bold indicates 95% significance. Units are percent.

	Rms ω	MSC amount	SST	SLP
Nimbostratus FQ	57/15/81	43/13/85	50/14/79	40/11/72
Rms ω		68/19/83	71/19/76	48/13/54
MSC amount			55/18/87	48/14/66
SST				57/17/66

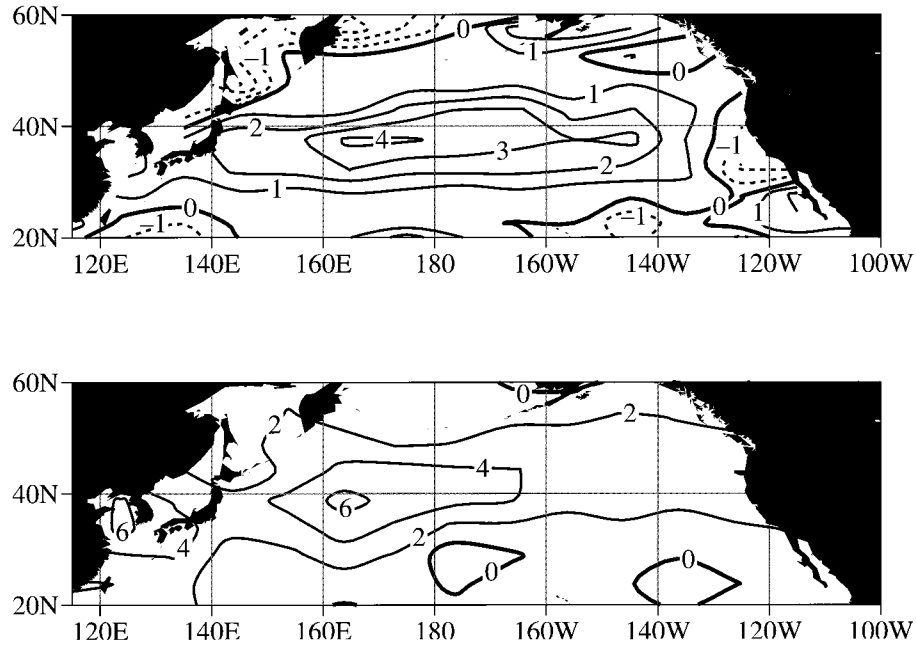


FIG. 6. Leading SVD patterns for (a) JJA daytime MSC amount paired with (b) JJA rms ω . Contour intervals are 1% (sky cover) and 2 mb day⁻¹; the zero contour is thickened and negative contours are dashed.

m; Batten 1972) allows significant changes in SST to occur on timescales less than a month. Correlations between MSC amount and SST exhibit much less lead-lag asymmetry than do correlations between rms ω and

SST. This suggests that boundary layer cloudiness primarily responds to SST and provides a positive feedback by changing surface insolation.

The character of atmosphere–ocean interaction in the

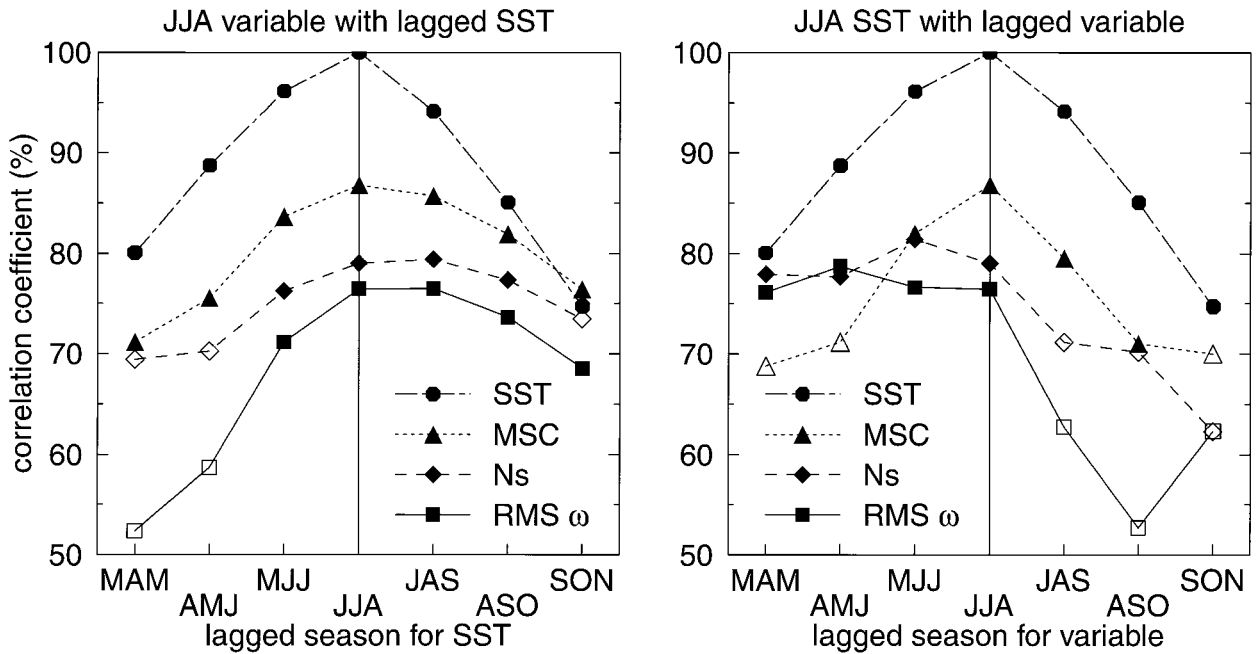


FIG. 7. (a) Correlation of SVD expansion coefficients (r) for SST, daytime MSC amount, daytime nimbostratus FQ, and rms ω during JJA paired with lagged 3-month average SST. (b) Correlation of SVD expansion coefficients (r) for SST during JJA with lagged 3-month average SST, daytime MSC amount, daytime nimbostratus FQ, and rms ω . Filled symbols indicate 95% significance.

North Pacific basin is very different between summer and winter. Summertime spatial patterns of variability in SST, rms ω , nimbostratus FQ, and MSC amount are zonal with nearly coincident centers of action. This suggests local processes operating in the storm track and over the SST gradient dominate interactions between the oceanic mixed layer, atmospheric boundary layer, and free atmosphere. Contrastingly, wintertime spatial patterns of SST, rms ω , nimbostratus FQ, and MSC amount do not have coincident centers of action and are not as closely coupled (not shown). Only relationships to mean SLP become stronger. This suggests the mean large-scale circulation and advection of cold continental air masses dominate interaction between the ocean and atmosphere.

5. Concluding remarks

The large correlation of leading rms ω with SST and the lack of sensitivity of atmospheric GCMs to midlatitude SST anomalies favors the hypothesis that the observed coupling between variability in the storm track and SST during summer primarily results from the atmosphere forcing the ocean. The resulting SST anomalies in turn modify the boundary layer and produce anomalies in MSC amount, which cause an additional positive feedback on SST. Variability in the storm track may also directly produce anomalies in MSC amount. Little relationship with the mean large-scale circulation is observed, probably because the lower continent-ocean temperature contrast during summer results in minimal exchange between atmosphere and ocean away from the SST gradient region.

If indeed it is the atmosphere primarily forcing the ocean, the question arises as to why parameters such as rms ω exhibit interdecadal variability. The limited memory of the atmosphere suggests that the observed trend in the storm track must be a response to forcing by some other part of the climate system. The ambiguous sensitivity of the atmosphere to midlatitude SST anomalies suggests it is not the midlatitude ocean. The Tropics seem a more likely candidate since the sensitivity of wintertime midlatitude atmospheric circulation to the tropical SST is well established (Lau and Nath 1994). Kawamura (1994) found an inverse relationship between midlatitude North Pacific SST and Indian Ocean SST during summer, but it is important to note this largely results from both regions having long-term trends. If a causal connection exists between tropical SST and the North Pacific storm track, it should also be seen in year-to-year variability. Examination of detrended SST data indicates that strong correlations with midlatitude North Pacific SST are generally confined to the region 5°S–15°N, 90°–120°E (not shown). The correlation between detrended JJA SST averaged over this region and the leading North Pacific EOF time series of detrended JJA rms ω is 0.46 (the unfiltered correlation is 0.47). Further investigation is needed to determine

whether changes in SST and convection in the eastern tropical Indian Ocean are responsible for the observed variability and long-term trend in the summertime North Pacific storm track.

Acknowledgments. This work was supported by the National Science Foundation while the author was an Advanced Study Program postdoctoral fellow at the National Center for Atmospheric Research. Preliminary work was supported by an Earth Observing System grant, NASA Grant NAGW-2633, while the author was a graduate student at the University of Washington. Chi-Fan Shih of the NCAR Data Support Section provided the reanalysis data. Clara Deser provided the 121-point bandpass filters. Doug Nychka suggested the method for dealing with autocorrelation. The author appreciates the comments of an anonymous reviewer.

APPENDIX

Calculation of Statistical Significance

SVD analysis is designed to maximize the covariance of the left and right fields and thus can create apparent coupling between two unrelated fields. The likelihood of spurious coupling can be estimated by randomly reordering the time series (the same at every grid point) separately for each field and applying SVD analysis. This preserves the spatial patterns in each field but removes correlation in time between them. Statistical significance of SCF, NC, or r is the percentage of 1000 pairs of reordered time series with SCF, NC, or r less than that of the real time series (only 100 pairs were used for Fig. 7).

The situation becomes more complex when autocorrelation is present. Random reordering removes autocorrelation from a time series; consequently, the real time series will have fewer effective temporal degrees of freedom than the simulated time series and statistical significance will be overestimated. The effect of autocorrelation at a grid point can be modeled by

$$x(t) = ax(t-1) + e(t), \quad (\text{A1})$$

where x is observed, t increments time, a is the autocorrelation, and values of e are temporally independent. Equation (A1) was used to calculate e at all grid points and times from the observed x and hence identify the distribution of variability not related to autocorrelation. These values of e were randomly reordered (the same at every grid point) and passed through A1 to obtain 1000 time series with the correct autocorrelation for the left and right fields. Statistical significance of SCF, NC, or r was then calculated as described above.

Statistical significance for correlations between the time series displayed in Fig. 3 was calculated by applying A1 and reordering each time series 1000 times. It is not necessary to reorder individual grid point time series since EOF analysis is conducted independently

on each field, and spatial information in one field need not be known by the other.

REFERENCES

- Bathen, K. H., 1972: On the seasonal changes in the depth of the mixed layer in the North Pacific ocean. *J. Geophys. Res.*, **77**, 7138–7150.
- Bottomley, M., C. K. Folland, J. Hsiung, R. E. Newell, and D. E. Parker, 1990: *Global Ocean Surface Temperature Atlas*. United Kingdom Meteorological Office and Massachusetts Institute of Technology, Department of Earth, Atmospheric, and Planetary Sciences, 20 pp. and 313 maps.
- Bretherton, C. S., C. Smith, and J. M. Wallace, 1992: An intercomparison of methods for finding coupled patterns in climate data. *J. Climate*, **5**, 541–560.
- Cess, R. D., and Coauthors, 1996: Cloud feedback in atmospheric general circulation models: An update. *J. Geophys. Res.*, **101**, 12 791–12 794.
- Ferranti, L., F. Molteni, and T. N. Palmer, 1994: Impact of localized tropical and extratropical SST anomalies in ensembles of seasonal GCM integrations. *Quart. J. Roy. Meteor. Soc.*, **120**, 1613–1645.
- Hahn, C. J., S. G. Warren, and J. London, 1995: The effect of moonlight on observation of cloud cover at night, and application to cloud climatology. *J. Climate*, **8**, 1429–1446.
- , —, and —, 1996: Edited synoptic cloud reports from ships and land stations over the globe, 1982–1991. Carbon Dioxide Information Analysis Center Rep. NDP026B, 45 pp. [Available from Carbon Dioxide Information Analysis Center, Oak Ridge National Laboratory, P. O. Box 2008, Oak Ridge, TN 37831-6335.]
- Hanson, H. P., 1991: Marine stratocumulus climatologies. *Int. J. Climatol.*, **11**, 147–164.
- Kalnay, E., and Coauthors, 1996: The NCEP/NCAR 40-Year Reanalysis Project. *Bull. Amer. Meteor. Soc.*, **77**, 437–471.
- Kawamura, R., 1994: A rotated EOF analysis of global sea surface temperature variability with interannual and interdecadal scales. *J. Phys. Oceanogr.*, **24**, 707–715.
- Klein, S. A., D. L. Hartmann, and J. R. Norris, 1995: On the relationships among low-cloud structure, sea surface temperature, and atmospheric circulation in the summertime northeast Pacific. *J. Climate*, **8**, 1140–1155.
- Kushnir, Y., and I. M. Held, 1996: Equilibrium atmospheric response to North Atlantic SST anomalies. *J. Climate*, **9**, 1208–1220.
- Lau, N.-C., and M. J. Nath, 1990: A general circulation model study of the atmospheric response to extratropical SST anomalies observed in 1950–1979. *J. Climate*, **3**, 965–989.
- , and —, 1994: A modeling study of the relative roles of tropical and extratropical SST anomalies in the variability of the global atmosphere–ocean system. *J. Climate*, **7**, 1184–1207.
- Norris, J. R., 1997: Interannual variability in cloudiness, sea surface temperature, and atmospheric circulation over the midlatitude North Pacific during summer. Ph.D. dissertation, University of Washington, 200 pp. [Available from University Microfilms, 1490 Eisenhower Place, P.O. Box 975, Ann Arbor, MI 48106.]
- , 1998: Low cloud type over the ocean from surface observations. Part II: Geographic and seasonal variations. *J. Climate*, **11**, 383–403.
- , and C. B. Leovy, 1994: Interannual variability in stratiform cloudiness and sea surface temperature. *J. Climate*, **7**, 1915–1925.
- , and —, 1995: Comments on “Trends in global marine cloudiness and anthropogenic sulphur.” *J. Climate*, **8**, 2109–2110.
- , Y. Zhang, and J. M. Wallace, 1998: Role of low clouds in summertime atmosphere–ocean interactions over the North Pacific. *J. Climate*, **11**, 2482–2490.
- Reiter, E. R., and D. R. Westhoff, 1982: Linear trends in Northern Hemisphere tropospheric geopotential height and temperature patterns. *J. Atmos. Sci.*, **39**, 528–541.
- Rozendaal, M. A., C. B. Leovy, and S. A. Klein, 1995: An observational study of diurnal variations of marine stratiform cloud. *J. Climate*, **8**, 1795–1809.
- Shabbar, A., K. Higuchi, and J. L. Knox, 1990: Regional analysis of Northern Hemisphere 50 kPa geopotential heights from 1946 to 1985. *J. Climate*, **3**, 543–557.
- Wallace, J. M., C. Smith, and C. S. Bretherton, 1992: Singular value decomposition of wintertime sea surface temperature and 500-mb height anomalies. *J. Climate*, **5**, 561–576.
- Warren, S. G., C. J. Hahn, J. London, R. M. Chervin, and R. L. Jenne, 1988: Global distribution of total cloud cover and cloud type amounts over the ocean. NCAR/TN-317+STR, Boulder, CO, 42 pp. and 170 maps. [Available from NCAR, P.O. Box 3000, Boulder, CO 80307.]
- Weare, B. C., 1994: Interrelationships between cloud properties and sea surface temperatures on seasonal and interannual time scales. *J. Climate*, **7**, 248–260.
- , and Coauthors, 1996: Evaluation of the vertical structure of zonally averaged cloudiness and its variability in the Atmospheric Model Intercomparison Project. *J. Climate*, **9**, 3419–3431.
- Weaver, C. P., and V. Ramanathan, 1996: The link between summertime cloud radiative forcing and extratropical cyclones in the North Pacific. *J. Climate*, **9**, 2093–2109.
- , and —, 1997: Relationships between large-scale vertical velocity, static stability, and cloud radiative forcing over Northern Hemisphere extratropical oceans. *J. Climate*, **10**, 2871–2887.
- Weng, F., N. C. Grody, R. Ferraro, A. Basist, and D. Forsyth, 1997: Cloud liquid water climatology from the Special Sensor Microwave/Imager. *J. Climate*, **10**, 1086–1098.
- Woodruff, S. D., R. J. Slutz, R. L. Jenne, and P. M. Steurer, 1987: A comprehensive ocean–atmosphere data set. *Bull. Amer. Meteor. Soc.*, **68**, 1239–1250.
- Zhang, Y., J. R. Norris, and J. M. Wallace, 1998: Seasonality of large scale atmosphere–ocean interaction over the North Pacific. *J. Climate*, **11**, 2473–2481.